JHEP|Reports

Bile acids attenuate hepatic inflammation during ischemia/reperfusion injury

Authors

Kunpeng Huang, Changyan Wang, Bosheng Mei, …, Peng Xu, Hui Wang, Jinxiang Zhang

Correspondence

zhangjinxiang@hust.edu.cn (J. Zhang), wanghuipitt@hust.edu.cn (H. Wang), m201875573@alumni.hust.edu.cn (K. Huang).

Graphical abstract

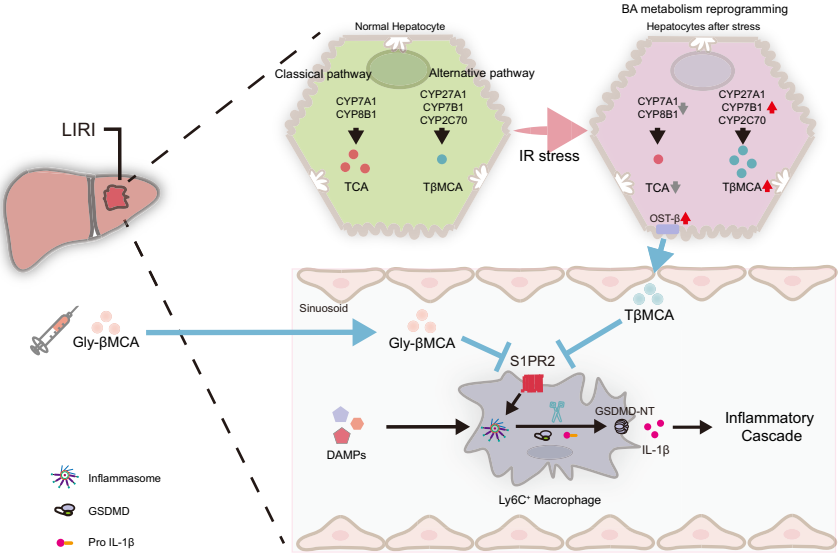

Highlights:

- Reprogramming of bile acid metabolism under liver ischemia/reperfusion stress attenuates liver injury.
- A shift in bile acid synthesis from the classical to the alternative pathway leads to increased TβMCA production.
- TβMCA reduces IL-1β release by inhibiting the macrophage S1PR2-GSDMD axis.
- Gly-βMCA, a derivative of TβMCA, attenuates inflammatory responses *in vivo* and *in vitro.*

Impact and implications:

Our research reveals that liver ischemia-reperfusion stress triggers reprogramming of bile acid metabolism. This functions as an adaptive mechanism to mitigate inflammatory injury by regulating the S1PR2-GSDMD axis, thereby controlling the release of IL-1β from macrophages. Our results highlight the crucial role of bile acids in regulating hepatocyte-immune cell crosstalk, which demonstrates an immunomodulatory function in liver reperfusion injury that may guide therapeutic strategies targeting bile acids and their receptors.

https://doi.org/10.1016/j.jhepr.2024.101101

Research article

JHEP|Reports

Bile acids attenuate hepatic inflammation during ischemia/reperfusion injury

Kunpeng Huang[1,2], Changyan Wang[3], Bosheng Mei[1], Jinglei Li[1], Tianxing Ren[1], Hanjing Zhan[4], Yunwei Zhang[5,6], Bowen Zhang[1], Xinyu Lv[1], Qi Zhang[1], Yong Guan[1], Xiaofei Zhang[7], Guoliang Wang[8], Wenming Pan[1], Peng Xu[1], Hui Wang[2,3,*], Jinxiang Zhang[1,2,*]

JHEP Reports **2024**. vol. 6 | 1–17

Background & Aims: Persistent cholestasis has been associated with poor prognosis after orthotopic liver transplantation. In this study, we aimed to investigate how the accumulation of tauro-beta-muricholic acid (TβMCA), resulting from the reprogramming of bile acid (BA) metabolism during liver ischemia/reperfusion (IR) stress, attenuates liver inflammation.

Methods: Ingenuity Pathway Analysis was performed using transcriptome data from a murine hepatic IR model. Three different models of hepatic IR (liver warm IR, bile duct separation-IR, common bile duct ligation-IR) were employed. We generated adeno-associated virus-transfected mice and CD11b-DTR mice to assess the role of BAs in regulating the myeloid S1PR2-GSDMD axis. Hepatic BA levels were analyzed using targeted metabolomics. Finally, the correlation between the reprogramming of BA metabolism and hepatic S1PR2 levels was validated through RNA-seq of human liver transplant biopsies.

Results: We found that BA metabolism underwent reprogramming in murine hepatocytes under IR stress, leading to increased synthesis of TβMCA, catalyzed by the enzyme CYP2C70. The levels of hepatic TβMCA were negatively correlated with the severity of hepatic inflammation, as indicated by the serum IL-1β levels. Inhibition of hepatic CYP2C70 resulted in reduced TβMCA production, which subsequently increased serum IL-1β levels and exacerbated IR injury. Moreover, our findings suggested that TβMCA could inhibit canonical inflammasome activation in macrophages and attenuate inflammatory responses in a myeloid-specific S1PR2-GSDMD-dependent manner. Additionally, Gly-βMCA, a derivative of TβMCA, could effectively attenuate inflammatory injury *in vivo* and inhibit human macrophage pyroptosis *in vitro*.

Conclusions: IR stress orchestrates hepatic BA metabolism to generate TβMCA, which attenuates hepatic inflammatory injury by inhibiting the myeloid S1PR2-GSDMD axis. Bile acids have immunomodulatory functions in liver reperfusion injury that may guide therapeutic strategies.

Introduction

Liver ischemia-reperfusion injury (IRI) is a sterile inflammatory response driven by innate immunity and represents a notable risk factor for liver transplantation.[1] Persistent postoperative cholestasis is closely related to poor prognosis in liver transplantation.[2–4] However, studies have shown that paradoxically, cholestasis can reduce tissue necrosis and inflammation severity in murine liver IRI.[5] Bile acids (BAs) are specific products of cholesterol and play important regulatory roles in both innate and adaptive immunity, their effects depend on their type and concentration.[6,7] Recent studies have suggested that BAs do not directly kill liver cells under pathophysiological conditions but rather induce pro-inflammatory genes in mouse and human hepatocytes.[8] However, the regulation of macrophage inflammasome activation through bile acid receptors (BARs), including farnesoid X receptor (FXR/NR1H4), or G-protein coupled bile acid receptor 1 (GPBAR1/TGR5) should still be considered based on current evidence.[9,10] Therefore, to fully understand the effects of BAs in the acute phase of hepatic IRI and how liver cells work synergistically and orchestrate BA metabolism to regulate sterile inflammation, further research is warranted.

Inflammasomes are a type of supramolecular organizing center that represent the signaling organelles of the innate immune system.[11] Inflammasome-mediated interleukin-1 beta (IL-1β) release is known to be important in liver inflammation.[12–14] Upon inflammasome assembly, Caspase-1 cleaves pro-IL-1β and gasdermin D (GSDMD) into active forms, GSDMD then releases its N-terminal fragment (GSDMD-NT) to form membrane pores, leading to hyperactive or pyroptotic cells.[15–18] Recent studies have indicated a link between BAs and inflammasome activation.[9,10] However, inconsistent data exist regarding whether BAs activate or inhibit inflammasome activation.[9,10,19,20] We hypothesized that BAs modulate liver IRI by regulating the inflammasome, while the type of BAs and the role of GSDMD in cell fate decisions needs to be considered.

Sphingosine 1-phosphate receptor 2 (S1PR2), a cell surface BAR, is known to be activated by taurocholic acid (TCA), a

* Corresponding authors. Address: 1277 Jiefang Road, Wuhan, Hubei Province 430022, China; Tel.: +8613638615196 (J. Zhang) or +8618995591866 (H. Wang).
E-mail addresses: zhangjinxiang@hust.edu.cn (J. Zhang), wanghuipitt@hust.edu.cn (H. Wang), m201875573@alumni.hust.edu.cn (K. Huang).
https://doi.org/10.1016/j.jhepr.2024.101101

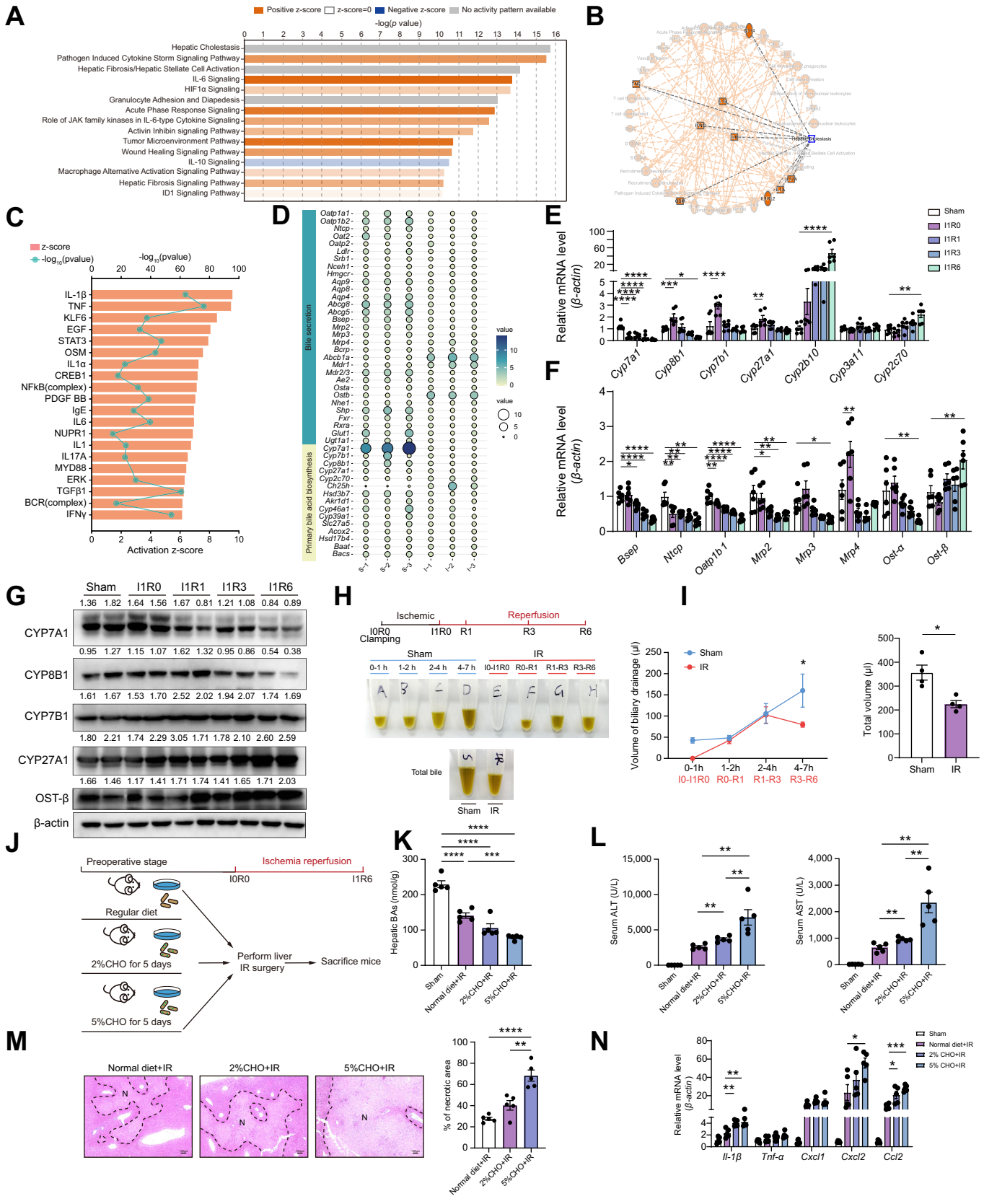

Fig. 1. IR orchestrates BA metabolism and participates in inflammatory injury. Sham and IR-stressed (ischemia for 1 h, reperfusion for 6 h) mouse liver lobes were subjected to transcriptome sequencing, followed by IPA (n = 3/group, DEG cut-offs: |log2FoldChange| >0.8, *p-adj* <0.1). (A) DEGs were used to perform canonical pathway analysis (the top 15 pathways of -log(*p*-value) are shown). (B) Correlation analysis between different molecules and enrichment pathways. (C) Upstream regulator prediction (the top 20 regulators of the activation z-score are shown). *p* values were calculated using Fisher's exact test. (D) Expression bubble map of genes

product of the classic BA synthesis pathway.[21,22] Studies have shown that hyperactive sphingosine-1-phosphate (S1P)/S1PR2 signaling enhances NLR family pyrin domain containing 3 (NLRP3) inflammasome activity and contributes to cholestatic liver injury.[23] Furthermore, S1PR2 promotes the formation of neutrophil extracellular traps and exacerbates liver IRI.[24] Interestingly, the liver's BA metabolic pathway can shift under pathological conditions, potentially regulating BAR activation[25,26] Thus, the interplay between BA metabolism and S1PR2 in sterile liver inflammation remains to be elucidated.

Herein, we report that tauro-beta-muricholic acid (TβMCA), an alternative BA synthesis product, alleviates liver inflammation by inhibiting myeloid-specific S1PR2, leading to reduced caspase-1/GSDMD-mediated IL-1β release. Our research suggests that BAs participate in GSDMD-mediated macrophage activation events under pathophysiological conditions and explains why BAs exhibit conflicting effects on inflammasome activation. These findings provide a novel therapeutic approach for targeting BAs and their receptors in liver diseases.

Materials and methods

Animals

All animal experiments were performed in compliance with institutional guidelines and approved by the Animal Care and Use Committee of Tongji Medical College (IACUC Number: 3442). C57BL/6 male wild-type mice were purchased from Vital River (Beijing, China), CD11b-DTR mice were kindly gifted by Prof. Congyi Wang, the Center for Biomedical Research, NHC Key Laboratory of Respiratory Diseases, Tongji Hospital, Huazhong University of Sciences and Technology, Wuhan, China, originally purchased from Shanghai Model Organisms.

Human studies

One public gene expression dataset (GSE151648) from human orthotopic liver transplant (OLT) biopsies was used to compare the transcriptome profiles of liver tissue between pre-transplantation (n = 23) and post-transplantation (n = 23) patients.[27] Needle-core liver biopsies from liver transplant recipients were obtained. We utilized this dataset for Ingenuity Pathway Analysis (IPA), and canonical pathways and upstream predictions were identified. GEO2R (GSE151648) was used to identify single-gene expression.

Classical mouse liver IR model and IR model with bile duct intervention

For the classical mouse liver IR model, partial hepatic ischemia-reperfusion was performed as previously described.[28] The abdomen was opened through a midline incision, and atraumatic microvascular clamps were used to interrupt the bile duct and the hepatic artery (HA)/portal vein (PV). After 60 min of partial (75%) ischemia, the clamps were removed, and the mice were sacrificed at 6 h of reperfusion. In the IR model with bile duct separation (BDS-IR), the bile duct was bluntly separated above the PV after exposure of the hepatic hilus. Vascular clamps were then placed to block the HA/PV. Following 60 min of ischemia, the clamps were removed, and the mice were sacrificed after 6 h of reperfusion. For the IR model with common bile duct ligation (CBDL-IR), the common bile duct was ligated above the pancreas with a 7-0 suture. Following this, a classical IR model was then operated. The CBDL model simply involves ligating the common bile duct after laparotomy without establishing an IR model.

Adoptive transfer experiments

To investigate the role of myeloid-specific S1PR2, we utilized a conditional depletion transgenic system in a CD11b-DTR mouse model. CD11b-DTR mice were pretreated intraperitoneally (i.p.) with diphtheria toxin (DT, 25 ng/g) 1 day before the experiment to deplete $CD11b^+$ native cells. Subsequently, 1 h before the IR surgery, mice were adoptively transferred with *in vitro*-generated bone marrow-derived macrophages (BMDMs; 5×10^5 cells i.v.) transfected with siRNA-control or siRNA-*S1pr2*.

For further details regarding the materials and methods used, please refer to the CTAT table and supplementary information.

Results

BA metabolism participates in the regulation of hepatic ischemia/reperfusion injury

To understand the molecular changes caused by IRI, we performed transcriptome sequencing on hepatic lobes of sham-operated and IR-stressed mice. A total of 18,493 differentially expressed genes (DEGs) were analyzed using IPA. IPA identified significant enrichment of the hepatic cholestasis pathway among the DEGs (-log(*p*-value) = 15.7, Fig. 1A; Table S1). This pathway exhibited a strong correlation with inflammatory

related to BA secretion and BA biosynthesis in sham and IR-stressed livers, value is the normalized FPKM data, S: sham; I: IR. (E) qRT-PCR analysis of BA synthesis-related gene expression in sham and IR-stressed livers (I1R0: ischemia for 1 h; I1R1: ischemia for 1 h, reperfusion for 1 h; I1R3: ischemia for 1 h, reperfusion for 3 h; I1R6: ischemia for 1 h, reperfusion for 6 h, n = 6/group). (F) qRT-PCR analysis of BA transporter expression in sham and IR-stressed livers (n = 6/group). (G) Western blot-assisted detection of CYP7A1, CYP8B1, CYP7B1, CYP27A1, and OST-β in sham and IR-stressed livers. (H-I) Bile ducts were intubated and draining bile was collected. Representative images of biliary drainage. The volume of bile was measured at different time points and the amount of bile was calculated (n = 4/group). (J) C57BL/6 mice were pretreated with cholestyramine (2% or 5%, w/w) or a normal diet before IR surgery, and liver/serum was collected after IR stress (n = 5/group). (K) BA levels in the liver. (L) Serum ALT/AST levels. (M) Representative H&E staining of liver sections. Percentages of necrotic areas were quantified (scale bar, 100 μm). (N) qRT-PCR analysis of pro-inflammatory gene expression in livers. Data are shown as mean±SEM. *p <0.05; **p <0.01; ***p <0.001; ****p <0.0001 by Student's t test or one-way ANOVA analysis. ALT, alanine aminotransferase; AST, aspartate aminotransferase; BA, bile acid; *Bsep* (*Abcb11*), bile salt export pump; CHO, cholestyramine; *Cyp7a1*, cholesterol 7α-hydroxylase; *Cyp8b1*, sterol 12α-hydroxylase; *Cyp7b1*, oxysterol 7α-hydroxylase; *Cyp27a1*, sterol 27-hydroxylase; *Cyp2b10*, cytochrome P450, family 2, subfamily b, polypeptide 10; *Cyp2c70*, cytochrome P450, family 2, subfamily c, polypeptide 70; IRI, ischemia-reperfusion injury; *Mrp2-4*, multidrug resistance associated protein 2-4; N, necrotic area; *Ntcp* (*Slc10a1*), sodium/taurocholate cotransporting polypeptide, solute carrier family 10, member 1; *Oatp1b1*, solute carrier organic anion transporter family, member 1B1; Ost-α/β, organic solute transporter alpha/beta; qRT-PCR, quantitative reverse-transcription PCR.

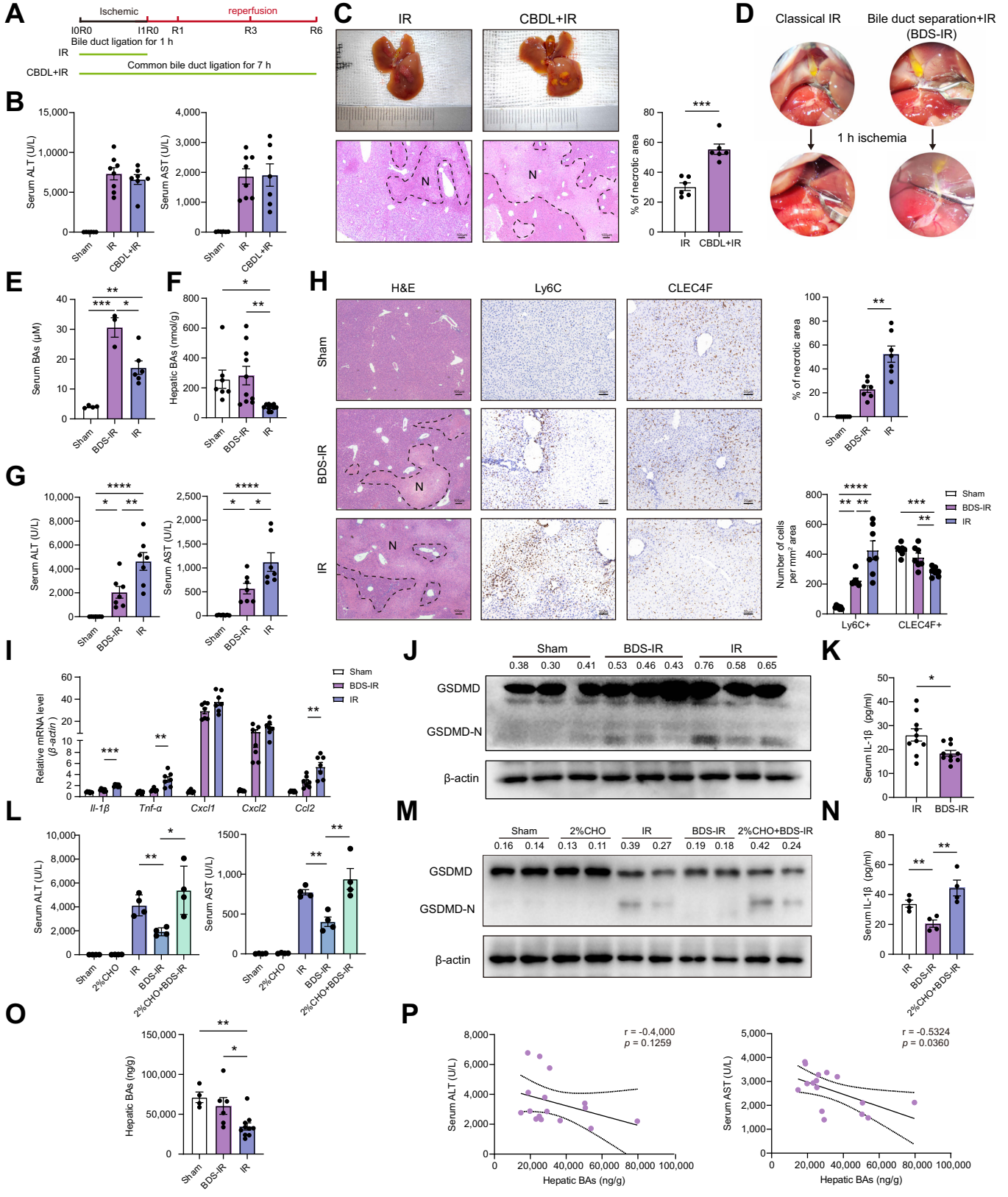

Fig. 2. Hepatic BAs attenuate murine IRI and inhibit IL-1β release. (A) C57BL/6 mice were subjected to IR or CBDL-IR stress, followed by liver/serum sampling after 6 h of reperfusion. (B) Serum ALT/AST levels (n = 6-8/group). (C) Liver tissue appearance and representative H&E staining of IR-stressed or CBDL-IR-stressed livers (n = 6/group). Percentages of necrotic areas in H&E staining were quantified (scale bar, 100 μm). (D) C57BL/6 mice were subjected to IR or BDS-IR stress, followed by liver/serum sampling after 6 h of reperfusion. Microscopic views before and after 1 h of ischemia. (E) Serum BA levels (n = 3-6/group). (F) Liver BA levels (n = 7-10/group). (G) Serum ALT/AST levels (n = 7/group). (H) Representative H&E and immunohistochemical staining of Ly6C$^+$ or CLEC4F$^+$ cells in liver

molecules, including IL-1β, IL-6, IFN-γ, and TNF-α (Fig. 1B). Among these, IL-1β showed the highest activity as an upstream regulator during the IR process (z-score = 9.558, p = 1.36E-64), followed by TNF-α (Fig. 1C, Table S2). IRI caused downregulation of several genes involved in BA metabolism. Specifically, *Cyp7a1* and *Cyp8b1* (involved in BA synthesis), *Ntcp* and *Oatp1b1* (responsible for hepatic basolateral uptake), *Bsep* and *Mrp2* (involved in canalicular export), and *Ost-α*, *Mrp3* and *Mrp4* (involved in the alternative basolateral efflux system) were all downregulated (Fig. 1D-F). In contrast, the BA detoxification enzymes *Cyp2b10* and 6β-hydroxylase *Cyp2c70*, as well as the basolateral transporter *Ost-β*, a gene involved in the export of taurine-conjugated BA into sinusoids,[29] increased significantly during the IR process (Fig. 1D-F). Interestingly, we also detected significant downregulation of CYP7A1 and CYP8B1, and upregulation of CYP27A1 and OST-β during the IR process at the protein level (Fig. 1G). The results of biliary drainage suggest a downregulation of bile excretion during reperfusion, and this may be a combined effect of altered bile acid synthesis and transport proteins (Fig. 1H,I).

To investigate the role of BAs in IRI regulation, cholestyramine was used to reduce hepatic BA levels (Fig. 1J). Cholestyramine pretreatment effectively reduced hepatic BA levels (Fig. 1K) and exacerbated IRI, as indicated by the elevated serum alanine aminotransferase (ALT)/aspartate aminotransferase (AST) levels (Fig. 1L), increased necrotic areas (Fig. 1M), and enhanced pro-inflammatory gene expression (Fig. 1N). Taken together, these findings suggest a regulatory role of BA metabolism in IR-induced hepatic inflammation.

Elevated hepatic BAs attenuate reperfusion injury and inhibit IL-1β release

While previous studies have suggested that CBDL can protect the liver from IRI by inducing cholestasis,[5] our study found no significant protective effect in the CBDL-IR group (Fig. 2A,B). However, there was a reduction in the expression of pro-inflammatory genes (Fig. S1A). Histological examination revealed biliary infarction and cholestatic necrosis in CBDL-IR-stressed livers (Fig. 2C). Interestingly, compared to the classical IR model, the BDS-IR model was associated with upregulated serum and hepatic BA levels (Fig. 2D-F), and protection from IR stress (Fig. 2G). Notably, BDS-IR stress decreased serum total cholesterol levels (Fig. S2A) while increasing serum total BA levels compared with IR stress (Fig. S2B). Immunostaining for the bile duct marker CK19 revealed bile duct contraction after IR stress, whereas bile duct dilatation was observed in the BDS-IR group (Fig. S2C). In addition, we detected upregulation of CK19 and ASBT expression in both IR-stressed and BDS-IR-stressed livers (Fig. S2D,E). Importantly, compared to IR stress, BDS-IR stress significantly reduced the infiltration of Ly6C$^+$ monocyte-derived macrophages (MoMFs), increased the presence of CLEC4F$^+$ liver-resident macrophages (Fig. 2H), and downregulated the expression of pro-inflammatory genes (Fig. 2I). As previously mentioned, IL-1β plays a crucial role in IRI regulation. We observed a significant reduction in hepatic GSDMD-N and serum IL-1β levels in the BDS-IR group (Fig. 2J,K). To further investigate the involvement of BAs in the protective effect against BDS-IR stress, we pretreated the mice with 2% cholestyramine to reduce BA levels. The beneficial effects of BDS-IR stress were abolished by cholestyramine pretreatment, as indicated by the restoration of serum ALT/AST, hepatic GSDMD-N, and serum IL-1β levels (Fig. 2L-N). Since hepatic homogenate BA levels usually reflect BA levels in pathophysiological conditions,[30] we conducted liquid chromatography-mass spectrometry analysis to determine hepatic BA levels in both IR and BDS-IR groups (Fig. 2O). Interestingly, a negative correlation between hepatic total BA and serum ALT/AST levels was observed (Fig. 2P). We also tested serum alkaline phosphatase (ALP) levels but found no correlation with serum ALT/AST levels (Fig. S2F,G). These results suggest that BDS-IR stress inhibits hepatic inflammatory injury by upregulating hepatic BA levels.

Metabolic reprogramming of hepatocytes promotes TβMCA production in the IR process

To identify the key BA profiles associated with liver protection during IRI, we compared the composition and concentration of BAs between BDS-IR-stressed and IR-stressed livers. Compared to the sham-operated group, the concentration of free BAs was decreased in both BDS-IR and IR stress groups. However, the BDS-IR model showed significantly higher levels of conjugated bile acids (CBAs), while the IR group showed similar CBA concentrations as the sham group (Fig. 3A). Notably, the levels of the primary hepatic BA TCA were decreased in the IR group, whereas TβMCA was elevated in the IR group and further increased in the BDS-IR group (Fig. 3B). Although the total CBAs and muricholic acids (MCAs) were reduced, TβMCA increased in the IR group, with its proportion in the MCA pool increasing from 6.16% to 24.23% and further increasing to 27.62% in the BDS-IR group (Fig. 3A-D). In contrast, the decrease in ω-MCA mainly contributed to the decline in free BAs and MCAs in IR-stressed livers (Fig. 3A,C-D). TβMCA was identified as the main endogenous BA in mice, derived from chenodeoxycholic acid (CDCA) in a reaction catalyzed by CYP2C70 (Fig. 3E).[31,32] Based on this, we hypothesized that both IR and BDS-IR stress induce metabolic reprogramming of BA biosynthesis. Our integrated analysis of transcriptomics and metabolism revealed a dominant alternative pathway activated in response to reperfusion injury

sections (n = 7/group). Percentages of necrotic areas and the number of Ly6C$^+$ or CLEC4F$^+$ cells were quantified (scale bar, 100 μm, and 50 μm). (I) qRT-PCR analysis of pro-inflammatory gene expression in the livers (n = 7/group). (J) Western blot-assisted detection and relative density ratio of GSDMD/GSDMD-NT. (K) Serum IL-1β levels (n = 10/group). (L) C57BL/6 mice were pretreated with 2% cholestyramine or a normal diet, followed by BDS-IR stress. Serum ALT/AST levels were measured (n = 4/group). (M) Western blot-assisted detection and relative density ratio of GSDMD/GSDMD-NT in the livers. (N) Serum IL-1β levels (n = 4/group). (O) BA-targeted metabolomic analysis in sham, BDS-IR-stressed, and IR-stressed livers (n = 4-10/group). Total liver BA levels were measured. (P) Correlations between total liver BAs and serum ALT/AST levels were analyzed by non-parametric Spearman's method (n = 16). Data are shown as mean±SEM. *p <0.05; **p <0.01; ***p <0.001; ****p <0.0001 by Student's t test or one-way ANOVA analysis. ALP, alkaline phosphatase; ALT, alanine aminotransferase; AST, aspartate aminotransferase; BDS-IR, bile duct separation with IR; CBDL, common bile duct ligation; CHO, cholestyramine; IRI, ischemia-reperfusion injury; MoMFs, monocyte-derived macrophages; N, necrotic area; qRT-PCR, quantitative reverse-transcription PCR; TBA, total bile acid.

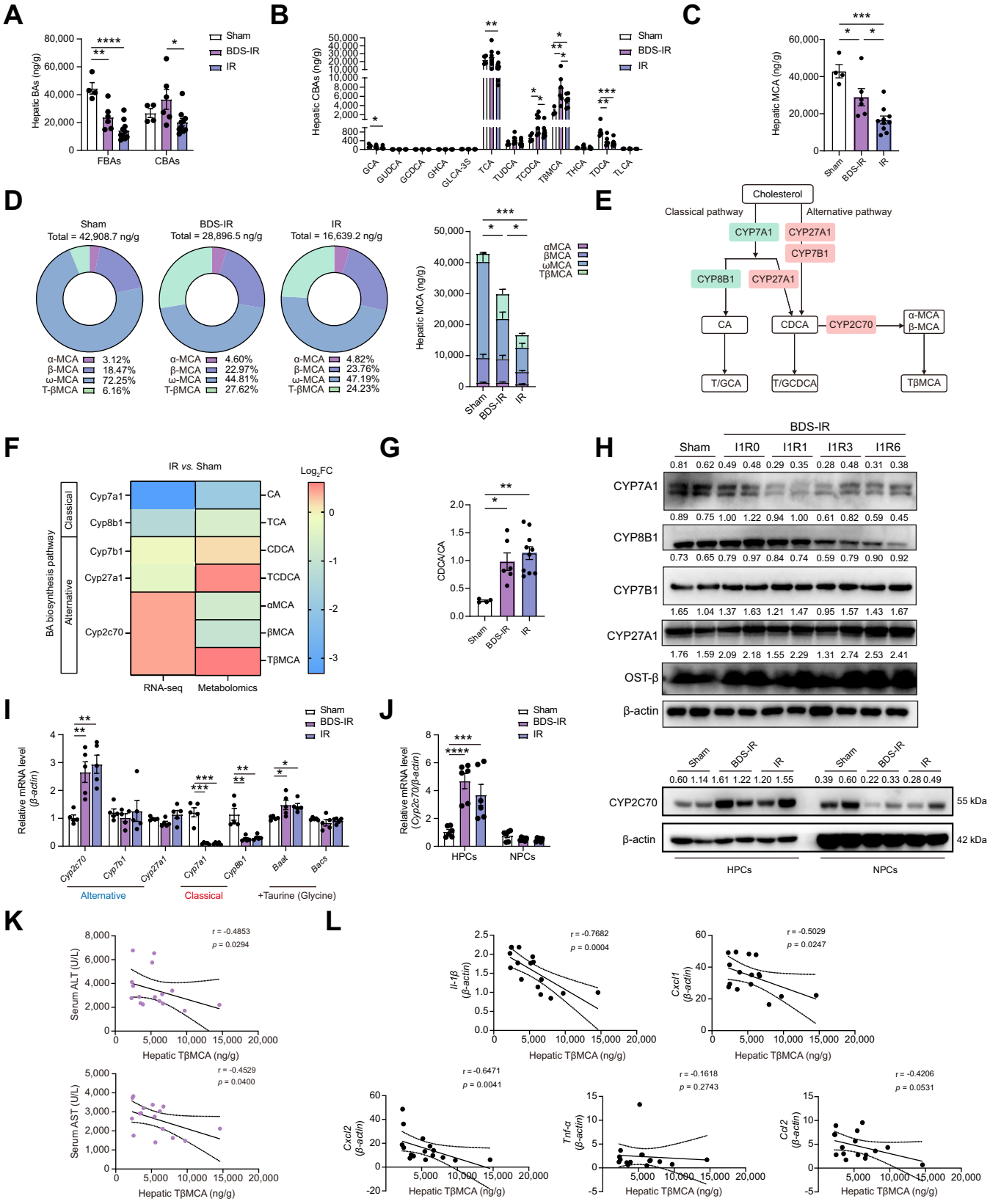

Fig. 3. IR induces metabolic pathway shifts to promote TβMCA production. C57BL/6 mice were subjected to IR or BDS-IR stress, and liver samples were obtained at 6 h of reperfusion for BA-targeted metabolomic analysis (n = 4-10/group). (A) Concentrations of FBAs and CBAs. (B) Concentrations of various CBAs. (C) Concentrations of MCAs. (D) Proportions and concentrations of different MCAs. (E) BA synthesis pathway in mice. (F) Combined transcriptomic and metabolomic analyses of the sham and IR-stressed livers. Significantly altered gene expression and bile acid levels after IR stress are shown. (G) Hepatic CDCA/CA ratio in sham, BDS-IR-stressed and IR-stressed livers. (H) C57BL/6 mice were subjected to BDS-IR stress, and liver samples were obtained at 0-6 h of reperfusion. Western blot-assisted

(Fig. 3F), as indicated by the increased CDCA/cholic acid ratio (Fig. 3G). The expression levels of genes related to BA metabolism exhibited similar patterns in the BDS-IR and IR groups (Figs 3H,I and S3A-C). These findings collectively suggest metabolic reprogramming of BAs in both BDS-IR-stressed and IR-stressed livers, with a notable increase in hepatic TβMCA levels as a unique feature.

CYP2C70 functions as a 6β-hydroxylase, converting CDCA to β-MCA. We observed a significant upregulation of CYP2C70 in hepatic primary cells of both BDS-IR and IR-stressed livers (Fig. 3J). Both BDS-IR and IR groups showed upregulation of *Baat*, which facilitated the conversion of β-MCA to TβMCA (Fig. 3I). Interestingly, we found a negative correlation between hepatic TβMCA levels and both serum ALT/AST levels (Fig. 3K), and hepatic pro-inflammatory gene expression (excluding *Tnf-a*) (Fig. 3L) in both IR and BDS-IR groups. These results indicated that IRI orchestrates BA metabolism to promote TβMCA production, which is negatively correlated with inflammation. Our findings suggest that the BDS-IR model can potentially potentiate this reprogramming and its protective effect.

CYP2C70-synthesized TβMCA alleviates IR-induced inflammatory injury

To investigate the role of CYP2C70 in regulating liver IRI, we utilized AAV8-sh*Cyp2c70* to reduce hepatic CYP2C70 levels (Fig. 4A,B). Unlike the progressive hepatic damage observed in *Cyp2c70*-knockout mice,[33] AAV8-sh*Cyp2c70* mice showed comparable body weights but an elevated liver-to-body weight ratio (Fig. 4C,D), while maintaining similar serum ALT/AST levels (Fig. 4E) and liver pathology (Fig. 4F) to the scrambled control (AAV8-control). However, while the expression of *Tnf-α*, *Cxcl1*, *Cxcl2*, and *Ccl2* remained comparable, hepatic *Il-1β* mRNA was significantly increased in AAV8-sh*Cyp2c70* mice compared to controls (Fig. 4G). Following the establishment of the IR model, AAV8-sh*Cyp2c70* mice displayed lower hepatic CYP2C70 expression and higher serum ALT/AST levels (Fig. 4H,I), along with increased necrotic areas in liver sections and pro-inflammatory gene expression (Fig. 4J,K). Moreover, AAV8-sh*Cyp2c70* mice exhibited higher hepatic GSDMD-NT and serum IL-1β levels after IR stress compared to control mice (Fig. 4L,M).

To determine the BA composition, we analyzed liver samples from different groups using liquid chromatography-mass spectrometry. Principal component analysis revealed distinct differences in BA profiles between AAV8-control and AAV8-sh*Cyp2c70* mice under IR stress (Fig. 4N). AAV8-sh*Cyp2c70* mice showed lower TβMCA levels (Fig. 4O) but elevated levels of CDCA and its derivatives, and these changes became more pronounced after IR stress (Fig. 4P,Q). To identify the key regulatory role of CYP2C70 in the BDS-IR model, we subjected AAV8-control and AAV8-sh*Cyp2c70* mice to both IR and BDS-IR models. Notably, under BDS-IR stress, AAV8-sh*Cyp2c70* mice displayed more severe liver damage compared to AAV8-control mice, as evidenced by increased serum ALT/AST and IL-1β levels. Furthermore, BDS-IR did not provide further protection beyond the effects observed in the IR group for AAV8-sh*Cyp2c70* mice (Fig. 4R,S). These results support the role of CYP2C70 in mediating the protective effect against IR via TβMCA production.

TβMCA inhibits macrophage-derived BA receptor S1PR2

BAs generally regulate immunometabolic functions through BARs, of which FXR and TGR5 are known for their anti-inflammatory properties.[7,9,10] IR stress led to a downregulation of hepatic FXR and its target genes, with an even more pronounced reduction observed in livers subjected to BDS-IR stress (Fig. S4A-D). Additionally, a similar inhibition of FXR was observed in hepatic primary cells, non-parenchymal cells, and macrophages and endothelial cells (Fig. S4E,F). While TGR5 expression was downregulated in IR-stressed and further downregulated in BDS-IR-stressed livers, upregulation of its downstream gene *Nos3* suggests that TGR5 may be activated during reperfusion (Fig. S4A-E,G). However, lower levels of both TGR5 and *Nos3* in BDS-IR-stressed livers indicated weaker activation of TGR5 compared to IR stress. Therefore, the BDS-IR model is unlikely to directly activate FXR or TGR5 to exert its protective effects.

We further investigated the expression of other BARs in both models (BDS-IR and IR). The expression of all examined BARs was comparable between BDS-IR and IR models, except for S1PR2, which showed significant downregulation in the BDS-IR group (Fig. 5A). In IR-stressed livers, S1PR2 expression increased after 1 h of ischemia but then returned to sham group levels by 6 h of reperfusion (Fig. S4H). However, BDS-IR stress led to a significant downregulation of S1PR2 in the liver (Figs S4I and 5B). Interestingly, S1PR2 expression was upregulated in sham-operated or IR-stressed livers of AAV-sh*Cyp2c70* mice (Fig. 5C). Immunohistochemical staining showed that CYP2C70 knockdown enhanced overall hepatic S1PR2 staining in sham and IR-stressed mice. Notably, strong S1PR2-positive staining was observed around necrotic areas in both IR-stressed control and AAV-sh*Cyp2c70* mice, but there was no significant increase in total S1PR2 protein levels after IR stress (Figs 5B-C and S5J). These findings are consistent with those observed in a mouse model of liver transplantation-mediated reperfusion injury,[24] and suggest a mechanism regulating S1PR2 during IR stress, which reduces overall hepatic S1PR2 levels.

To determine whether S1PR2 plays a role in IR-induced inflammatory injury, we conducted *in vivo* experiments. Our results demonstrated that the S1PR2-inhibitor JTE-013

detection and relative density ratio of CYP7A1, CYP8B1, CYP7B1, CYP27A1, and OST-β in the sham and BDS-IR-stressed livers. (I) qRT-PCR analysis of BA synthesis-related gene expression in sham, BDS-IR-stressed, and IR-stressed livers (n = 5/group). (J) HPCs and NPCs were isolated from BDS-IR-stressed and IR-stressed livers, qRT-PCR analysis of *Cyp2c70* levels (n = 6/group). Western blot-assisted detection and relative density ratio of CYP2C70. (K, L) Correlations between hepatic TβMCA levels and serum ALT/AST levels, as well as *Il-1β*, *Cxcl1*, *Cxcl2*, *Ccl2* and *Tnf-α* levels were analyzed by non-parametric Spearman's method (n = 16). Data are shown as mean±SEM. *p <0.05; **p <0.01; ***p <0.001; ****p <0.0001 by one-way ANOVA analysis. ALT, alanine aminotransferase; AST, aspartate aminotransferase; BAs, bile acids; BDS-IR, bile duct separation with IR; CBAs, conjugated bile acids; FBAs, free bile acids; HPCs, hepatic primary cells; IR, ischemia-reperfusion; LC-MS, liquid chromatography-mass spectrometry; MCAs, muricholic acids; NPCs, non-parenchymal cells; qRT-PCR, quantitative reverse-transcription PCR.

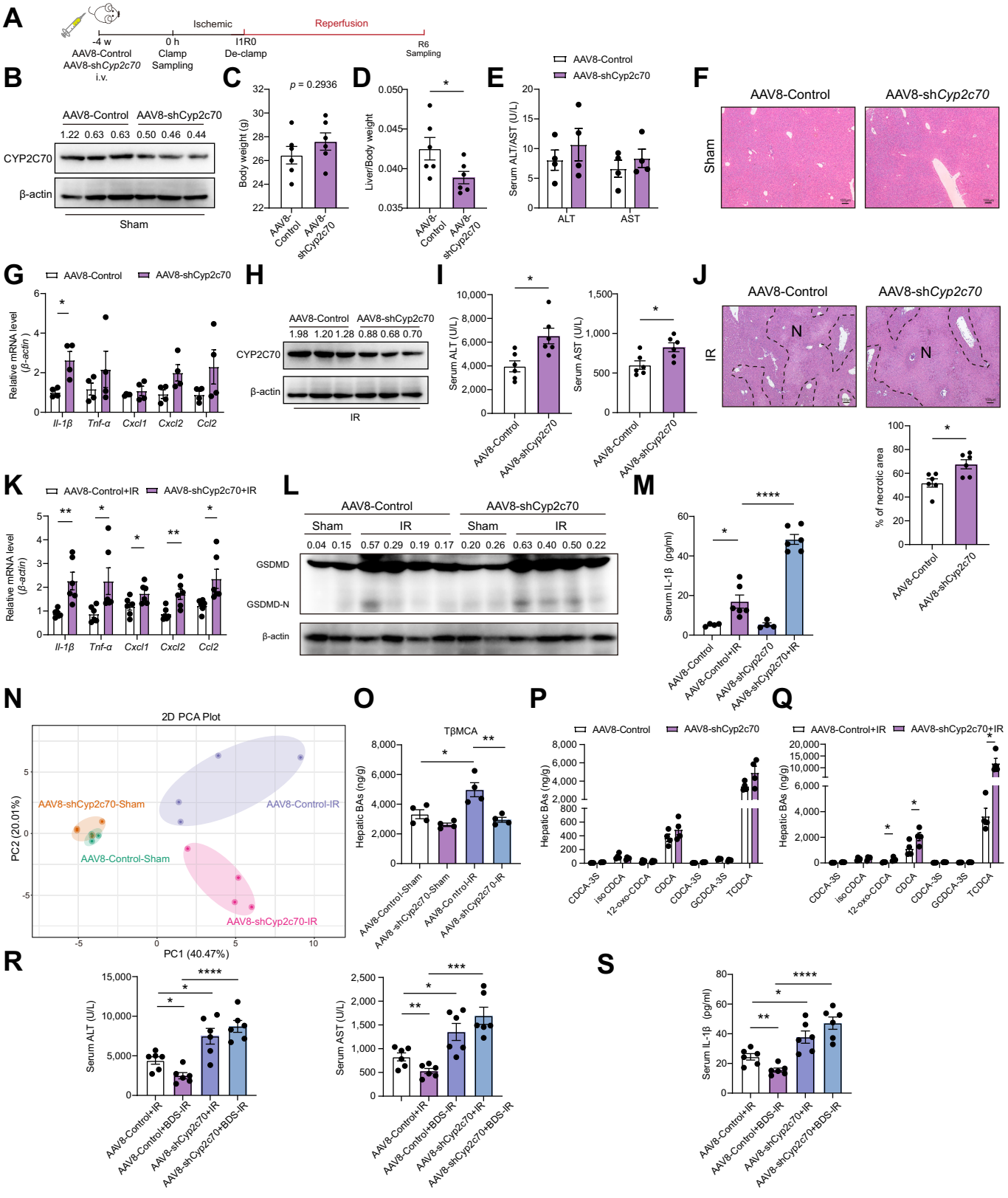

Fig. 4. Inhibition of hepatic *Cyp2c70* exacerbates IR inflammatory injury. (A) AAV8-*Cyp2c70*-shRNA was used to generate CYP2C70 knockdown mice (AAV-sh*Cyp2c70*). AAV8-*Cyp2c70*-shRNA was injected into 6-week-old mice for 4 weeks, followed by liver/serum sampling. (B) Western blot-assisted detection and relative density ratio of CYP2C70 in sham-operated AAV8-control and AAV8-sh*Cyp2c70* mice. (C) Body weight measurements (n = 6/group). (D) Ratio of the liver-to-body weight (n = 6/group). (E) Serum ALT/AST levels (n = 4/group). (F) Representative H&E staining in liver sections. (G) qRT-PCR analysis of *Il-1β*, *Tnf-α*, *Cxcl1*, *Cxcl2*, and *Ccl2* levels in the livers (n = 4/group). (H) AAV8-control and AAV8-*shCyp2c70* mice were subjected to IR stress, followed by liver/serum sampling after 6 h of reperfusion (n = 6/group). Western blot-assisted detection and relative density ratio of CYP2C70 in IR-stressed AAV8-control and AAV8-sh*Cyp2c70* mice. (I) Serum

effectively decreased serum ALT/AST and serum IL-1β levels in IR-stressed mice (Fig. 5D-F). JTE-013 injection after ischemia showed greater protection and improved pathology (Fig. 5E-G). To identify the main cell types regulated by S1PR2, we successfully overexpressed *S1pr2* in the liver using AAV (AAV8-oe*S1pr2*) (Fig. S5A-C). Interestingly, IR-stressed AAV8-oe*S1pr2* mice did not exhibit worse liver injury compared to AAV8-control mice (Fig. S5D-F). Using GdCl3 to deplete hepatic resident macrophages and inhibit MoMF infiltration,[34] we found that both AAV8-control and AAV8-oe*S1pr2* mice were protected from IR stress (Fig. S5F). Importantly, isolated non-parenchymal cells showed significant downregulation of *S1pr2* in the IR group and a further decrease in the BDS-IR group, whereas hepatic primary cells showed consistent expression of *S1pr2* (Fig. 5H). Our analysis of hepatic M1/M2 macrophage polarization under IR and BDS-IR stress revealed that BDS-IR stress significantly inhibited M1 polarization (Fig. S6). Immunofluorescence analysis indicated that S1PR2 was mainly localized in Ly6C$^+$ MoMFs but not in CLEC4F$^+$ Kupffer cells in both BDS-IR and IR-stressed livers (Fig. 5I-L). These findings suggest that S1PR2 may primarily play a pro-inflammatory role through MoMFs during IRI. Furthermore, we treated mouse primary BMDMs with various BAs whose levels changed after IR and BDS-IR stress. We found that cholic acid, CDCA, TCA, and ω-MCA increased *S1pr2* expression, whereas ursodeoxycholic acid (UDCA), αMCA, and TβMCA inhibited it, with TβMCA exerting the strongest inhibitory effect (Fig. 5M). Indeed, under inflammasome-activated conditions, TβMCA inhibited S1PR2 expression and its downstream signaling molecules, p-AKT1 and p-ERK1/2 (Fig. 5N). These results confirm the significant suppressive effect of TβMCA on S1PR2 expression in macrophages.

Myeloid S1PR2 exacerbates hepatic IR injury via GSDMD-regulated IL-1β release

To investigate whether TβMCA could regulate macrophage pyroptosis and IL-1β release, BMDMs were treated with different doses of TβMCA, followed by lipopolysaccharide (LPS)/ATP stimulation. TβMCA inhibited Caspase-1-p20/GSDMD-NT levels, IL-1β and lactate dehydrogenase (LDH) release in a concentration-dependent manner (Fig. 6A,B). Interestingly, TCA and ω-MCA, which increased S1PR2 expression in macrophages, also promoted GSDMD cleavage and IL-1β release (Fig. S7A-D). Upon IR stress, both TCA and ω-MCA levels notably decreased (Fig. 3B, D), suggesting that IR-induced reprogramming of BA metabolism may shift pro-pyroptotic BAs towards anti-pyroptotic BAs.

To investigate whether S1PR2 regulates pyroptosis, we treated BMDMs with the S1PR2 inhibitor JTE-013 or the agonist CYM-5520, followed by LPS/ATP stimulation. Notably, JTE-013 significantly reduced caspase-1-p20/GSDMD-NT levels as well as IL-1β and LDH release, whereas CYM-5520 exacerbated pyroptosis (Fig. 6C,D). However, longer treatments (Fig. S8A,B) or higher concentrations (Fig. S8C,D) of CYM-5520 reduced caspase-1-p20/GSDMD-NT levels and IL-1β release but increased LDH levels. This aligns with previous studies showing that pyroptotic cells release lower levels of IL-1β but higher LDH levels compared to hyperactivated macrophages. Disulfiram has been reported to inhibit GSDMD oligomerization without affecting its cleavage in THP-1 cells, thereby inhibiting pyroptosis.[35] We treated phorbol 12-myristate 13-acetate-differentiated and LPS-primed THP-1 with different doses of CYM-5520, followed by disulfiram/ATP stimulation. As expected, CYM-5520 promoted GSDMD cleavage in a dose-dependent manner while inhibiting pyroptosis (Fig. S8E-G). Interestingly, injection of low-dose CYM-5520 before ischemia significantly worsened IRI and increased serum IL-1β levels, whereas high-dose CYM-5520 did not induce this effect (Fig. S8H-J). Instead, high-dose CYM-5520 reduced serum ALT/AST levels at 3 h of reperfusion (Fig. S8K, L). Collectively, these results highlight the role of macrophage S1PR2 in promoting GSDMD activation and IL-1β release.

To determine whether TβMCA regulates pyroptosis via macrophage S1PR2, molecular docking simulations were conducted using CB-Dock2 to analyze how different compounds interact with S1PR2.[36] The software docked synthetic compounds (CYM-5520, JTE-013) and natural ligands (TCA, ω-MCA, and TβMCA) to specific binding pockets on S1PR2 (Figs 6E and S9A). Notably, TβMCA and JTE-013 shared overlapping binding sites and interaction residues (Fig. 6E). Subsequently, siControl-BMDMs and siS1pr2-BMDMs were treated with various doses of TβMCA, followed by LPS/ATP stimulation. The results demonstrated that silencing S1PR2 diminished the inhibitory effect of TβMCA on pyroptosis (Fig. 6F,G). To better understand how S1PR2 regulates macrophage pyroptosis, we treated BMDMs with JTE-013, CYM-5520, or vehicle control, followed by LPS/ATP stimulation. RNA sequencing was conducted on these cells, and DEGs were analyzed in the JTE-013 *vs*. control or CYM-5520 *vs.* control groups using IPA. We identified several pathways that were inhibited by JTE-013 but activated by CYM-5520, including the IL-1 family signaling and pyroptosis pathways (Fig. 6H). Furthermore, the genes enriched in the pyroptosis pathway suggested that pyroptosis-related genes were downregulated in JTE-013 *vs.* control and upregulated in CYM-5520 *vs.* control (Fig. S9B). These results support the hypothesis that TβMCA inhibits pyroptosis through S1PR2.

To identify the role of myeloid S1PR2 in mediating IRI, we employed a CD11b-DTR adoptive transfer mouse model.[37]

ALT/AST levels. (J) Representative H&E staining of liver sections (n = 6/group). Percentages of necrotic areas were quantified (scale bar, 100 μm). (K) qRT-PCR analysis of *Il-1β, Tnf-α, Cxcl1, Cxcl2,* and *Ccl2* levels in the livers (n = 6/group). (L) AAV-control and AAV-sh*Cyp2c70* mice were subjected to IR stress, followed by liver/serum sampling after 6 h of reperfusion. Western blot-assisted detection and relative density ratio of GSDMD/GSDMD-NT in the livers. (M) Serum IL-1β levels (n = 4-6/group). (N) BA-targeted metabolomic analysis in sham or IR-stressed livers of AAV-control/AAV-sh*Cyp2c70* mice (n = 4/group). Global sample distribution profiles were analyzed by the PCA. (O) Abundance of TβMCA in each group. (P-Q) Abundance of CDCA and its derivatives in sham and IR groups. (R) IR and BDS-IR models were established in AAV-control/AAV-sh*Cyp2c70* mice, followed by liver/serum sampling after 6 h of reperfusion (n = 6/group). Serum ALT/AST levels. (S) Serum IL-1β levels. Data are shown as mean±SEM. **p* <0.05; ***p* <0.01; ****p* <0.001; *****p* <0.0001 by Student's *t* test. AAV, adeno-associated virus; ALT, alanine aminotransferase; AST, aspartate aminotransferase; BA, bile acid; BDS-IR, bile duct separation with IR; IR, ischemia-reperfusion; LC-MS, liquid chromatography-mass spectrometry; N, necrotic area; PCA, principal component analysis; qRT-PCR, quantitative reverse-transcription PCR.

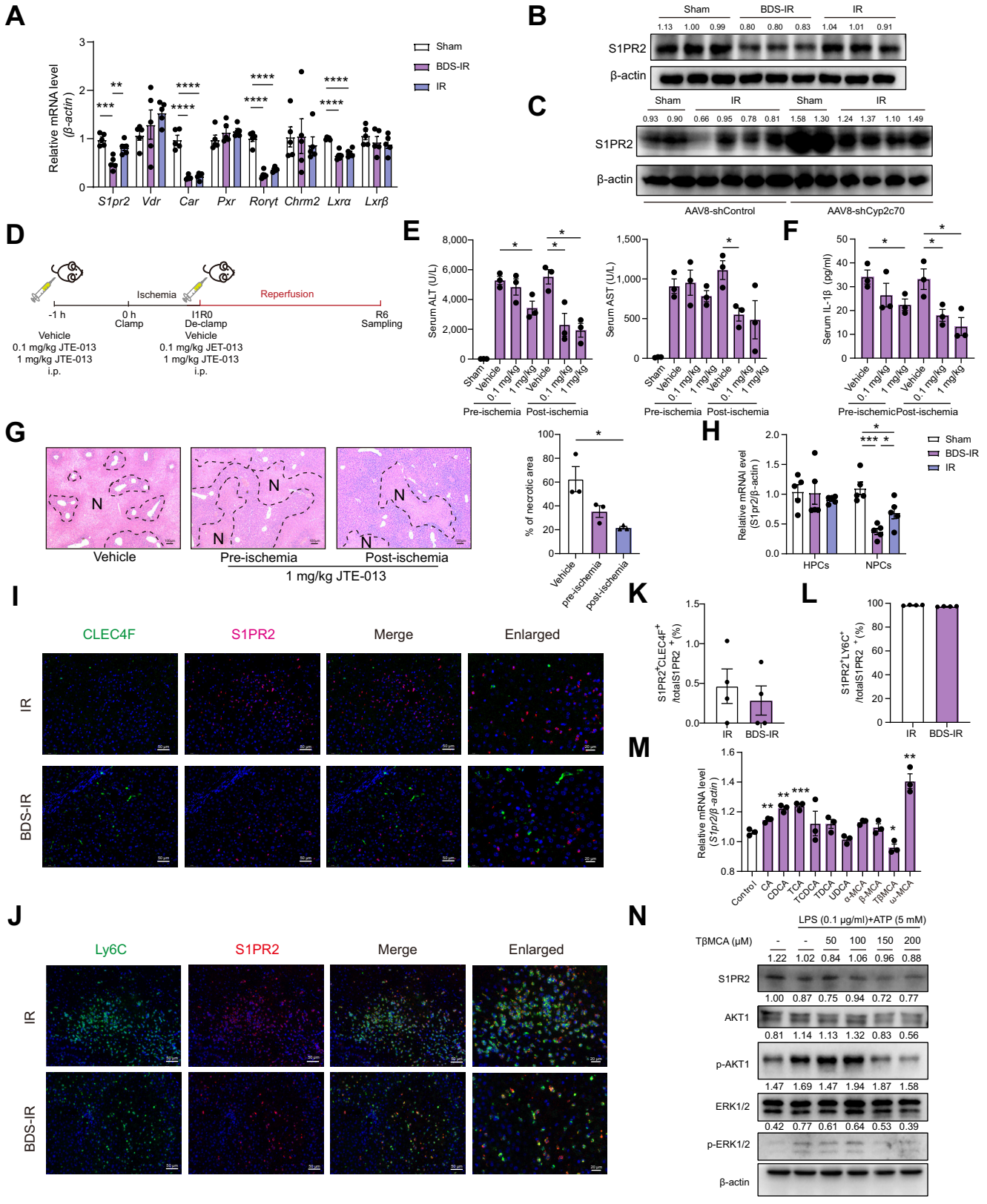

Fig. 5. TβMCA inhibits BA receptor S1PR2 in Ly6C$^+$ macrophages. C57BL/6 mice were subjected to IR or BDS-IR stress, followed by liver/serum sampling after 6 h of reperfusion. (A) Expression of different BA receptors including *S1pr2, Vdr, Car, Pxr, Rorγt, Chrm2, Lxrα* and *Lxrβ* were detected by qRT-PCR (n = 5/group). (B) Western blot-assisted detection and relative density ratio of S1PR2 in the sham, BDS-IR-stressed, and IR-stressed livers. (C) Western blot-assisted detection and relative density ratio of S1PR2 in sham or IR-stressed livers of AAV-control/AAV-sh*Cyp2c70* mice. (D) C57BL/6 mice were treated with JTE-013 (0.1 mg/kg, or 1 mg/kg) or vehicle 1 h before ischemia (pre-ischemia) or at the beginning of reperfusion (pre-reperfusion), followed by liver/serum sampling after 6 h of reperfusion. (E-F) Serum ALT/AST and IL-1β levels (n = 3/group). (G) Representative H&E staining of liver sections (n = 3/group). Percentages of necrotic areas were quantified (scale bar,

Following depletion of CD11b$^+$ cells using DT pretreatment (25 ng/g i.v., day-1), mice were re-infused with either siControl-BMDMs or si*S1pr2*-BMDMs 1 h before the IR procedure (Fig. 6I). Infusion of si*S1pr2*-BMDMs resulted in significant reductions in serum ALT/AST levels (Fig. 6J), hepatic *S1pr2* expression (Fig. 6K), necrotic areas in liver sections (Fig. 6L) and pro-inflammatory gene expression (Fig. 6M), as well as hepatic GSDMD-N and serum IL-1β levels, when compared to siControl-BMDMs infusion (Fig. 6N,O). These results indicate that TβMCA attenuates IR-induced inflammatory responses by negatively regulating the myeloid-specific S1PR2-GSDMD axis.

Gly-βMCA attenuates IR inflammatory injury and inhibits human macrophage pyroptosis

Glycine-βMCA (Gly-βMCA), a derivative of TβMCA, has been shown to improve metabolic dysfunction-associated steatohepatitis.[38,39] Similar to TβMCA, Gly-βMCA bound to S1PR2 (Fig. 7A). Moreover, Gly-βMCA significantly inhibited LPS/ATP-induced pyroptosis in BMDMs and reduced S1PR2, p-AKT1, and p-ERK1 levels (Fig. 7B,C). Although a 200 μM dose of Gly-βMCA may harm mouse macrophages, IL-1β and LDH levels were still lower than in the control group (Fig. 7C). High-dose treatment with Gly-βMCA in THP-1 cells maintained its effectiveness in inhibiting pyroptosis (Fig. 7D,E). Similarly, S1PR2 silencing in macrophages diminished the inhibitory effects of Gly-βMCA on pyroptosis (Fig. 7F, G), confirming that the anti-inflammatory effect of Gly-βMCA depends on S1PR2 in macrophages.

Next, we investigated the therapeutic effects of Gly-βMCA in mice. Mice received varying doses of Gly-βMCA intravenously 1 h before IR surgery (Fig. 7H). This resulted in a dose-dependent reduction in serum ALT/AST levels (Fig. 7I), pro-inflammatory gene expression (Fig. 7J), and necrotic areas in liver sections observed at 6 h of reperfusion (Fig. 7K). Interestingly, in the necrotic areas of liver sections with similar infiltration of Ly6C$^+$ MoMFs, Gly-βMCA treatment induced a dose-dependent decrease in S1PR2 levels (Fig. 7K). Additionally, Gly-βMCA-treated mice showed reduced levels of hepatic S1PR2, GSDMD-N, and serum IL-1β (Fig. 7L,M). These findings indicate that Gly-βMCA inhibits the expression of S1PR2 in Ly6C$^+$ MoMFs and the release of IL-1β mediated by GSDMD, ultimately resulting in a protective effect against IRI.

To determine the significance of the BA-mediated myeloid S1PR2-GSDMD axis in human liver IRI, we analyzed RNA-seq data from a public dataset (GSE151648) involving human OLT patients.[27] Analysis of DEGs between pre- and post-transplant liver samples revealed enrichment in innate immune signaling pathways (Fig. S10A, Table S3). Upstream analysis identified TNF, IFN-γ, and IL-1β as key regulators (Fig. S10B, Table S4). Human IR stress induced upregulation of *IL-1β, CCL2,* and *IL-6* expression (Fig. S10C), while downregulating *CYP27A1* (Fig. S10D). Importantly, human OLT samples displayed elevated S1PR2 expression, suggesting a potential lack of BA-mediated S1PR2 inhibition during human IR stress (Fig. S10E). This highlights the potential of targeting myeloid S1PR2 with Gly-βMCA as a therapeutic strategy for human OLT.

Discussion

This study investigated the role of TβMCA-S1PR2 signaling in regulating the canonical inflammasome pathway in macrophages. During IR stress, TβMCA levels significantly increase when transitioning to an alternative pathway for BA synthesis. We showed that TβMCA reduced macrophage IL-1β release by inhibiting S1PR2-mediated caspase-1/GSDMD activation. In contrast, TCA, a product of the classical BA synthesis pathway, activates the inflammasome. Analysis of RNA-seq data from human OLT biopsies revealed a potential lack of BA-mediated suppression of myeloid S1PR2-mediated inflammasome activation during human IR stress. Therefore, Gly-βMCA, which inhibits the macrophage S1PR2-GSDMD axis, could be a potential therapeutic target.

Our study revealed a novel pathway linking BA metabolism to inflammation in mice subjected to IR stress. We demonstrated that hepatic BAs suppress inflammation during IR using cholestyramine treatment and our established BDS-IR model. While the CBDL+IR model reduced inflammatory factors, it did not attenuate serum ALT/AST levels. This might be due to increased hepatocyte injury from biliary infarction during reperfusion (Figs S1 and 2B). In contrast, the BDS-IR model induces moderate extrahepatic bile duct obstruction, leading to a modest rise in BA levels instead of persistent blockage. Notably, serum ALP levels were not significantly elevated in the BDS-IR group and did not correlate with serum ALT/AST levels (Fig. S2F,G). We hypothesize that despite elevating bile duct pressure and intrahepatic BA levels, the BDS-IR model causes less severe disruption of the bile-blood barrier and inhibits ALP elevation due to its attenuating effect on inflammation during reperfusion. This validates earlier research indicating that BAs do not exacerbate inflammatory injury but rather attenuate hepatic inflammation during IR.[5] We identified TβMCA as a protective metabolite, which showed a negative correlation with hepatic inflammation. Furthermore, CYP2C70 knockdown in hepatocytes exacerbates IR injury, while an analog of

100 μm). Vehicle: injection of vehicle at the beginning of reperfusion. (H) qRT-PCR analysis of *S1pr2* levels in HPCs and NPCs isolated from sham, BDS-IR-stressed, and IR-stressed livers (n = 5/group). (I) Representative immunofluorescence staining of CLEC4F (green), S1PR2 (red), merged, and enlarged images of IR-stressed or BDS-IR-stressed livers (scale bar, 50 and 20 μm). (J) Representative immunofluorescence staining of Ly6C (green), S1PR2 (red), merged, and enlarged images of IR-stressed or BDS-IR-stressed livers (scale bar, 50 and 20 μm). (K) The percentages of S1PR2$^+$ CLEC4F$^+$ cells were quantified (n = 4/group). (L) The percentages of S1PR2$^+$ Ly6C$^+$ cells were quantified (n =4/group). Scale bars, 50 and 20 μm. (M) Mouse BMDMs were treated with CA, CDCA, TCA, TCDCA, TDCA, UDCA, αMCA, βMCA, TβMCA, ω-MCA (50 μM), or DMSO for 3 h. qRT-PCR analysis of *S1pr2* levels in cell lysates (n =3/group). (N) BMDMs were treated with LPS (0.1 μg/ml) and TβMCA (0, 50, 100, 150 or 200 μM) for 3 h, followed by ATP treatment (5 mM, 0.5 h). Western blot-assisted detection and relative density ratio of S1PR2, AKT1, p-AKT1, ERK1/2, and p-ERK1/2 in cell lysates. Data are shown as mean±SEM. *p <0.05; **p <0.01; ***p <0.001; ****p <0.0001 by Student's t test or one-way ANOVA analysis. AAV, adeno-associated virus; ALT, alanine aminotransferase; AST, aspartate aminotransferase; BAs, bile acids; BARs, bile acid receptors; BDS-IR, bile duct separation with IR; BMDMs, bone marrow-derived macrophages; HPCs, hepatic primary cells; IR, ischemia-reperfusion; KCs, Kupffer cells; LPS, lipopolysaccharide; LSECs, liver sinusoidal endothelial cells; MoMFs, monocyte-derived macrophages. N, necrotic area; NPCs, non-parenchymal cells; qRT-PCR, quantitative reverse-transcription PCR.

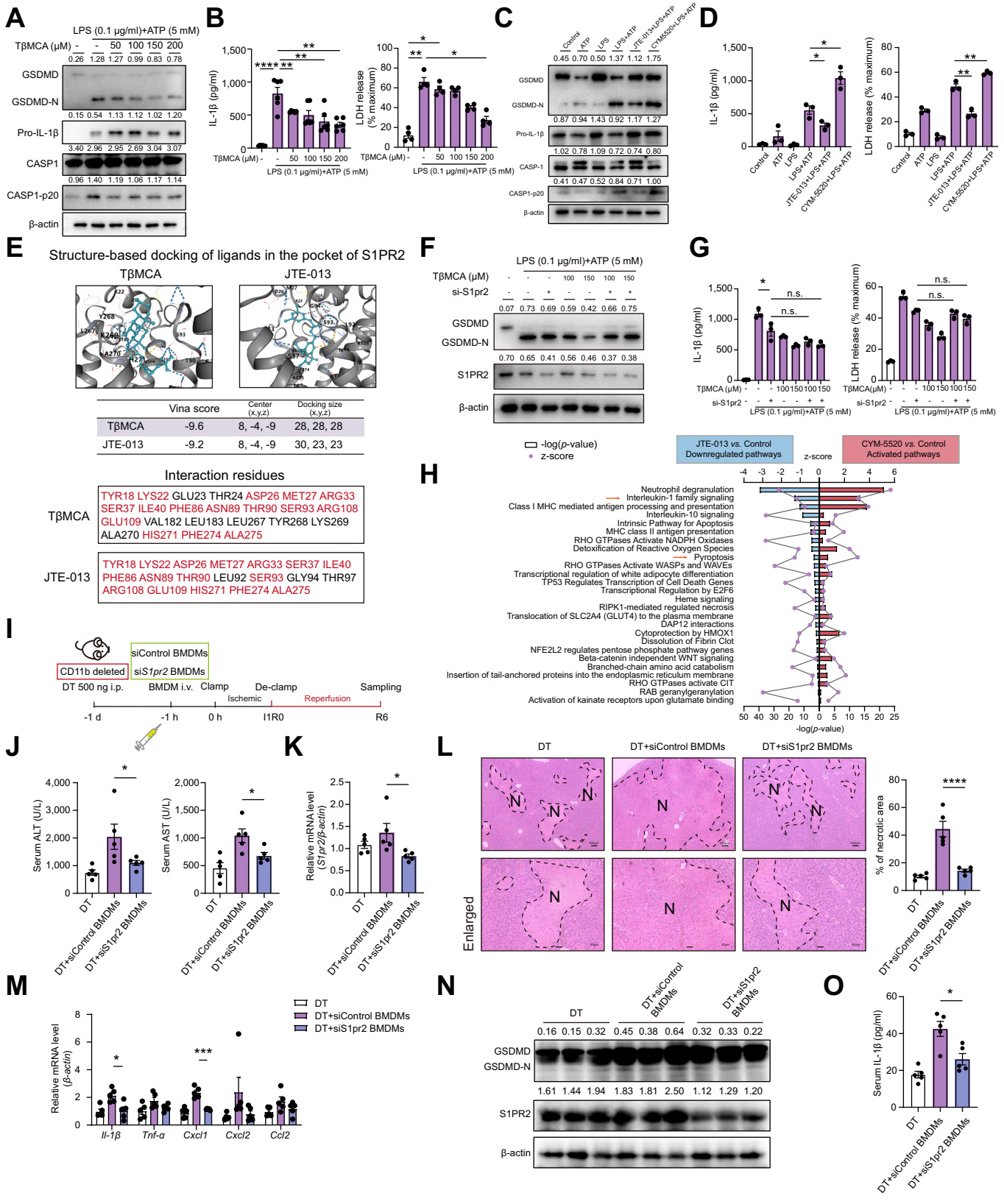

Fig. 6. TβMCA inhibits myeloid macrophage-specific S1PR2-GSDMD-mediated IL-1β release. (A) BMDMs were treated with LPS (0.1 μg/ml) and TβMCA (0, 50, 100, 150 or 200 μM) for 3 h, followed by ATP treatment (5 mM, 0.5 h). Western blot-assisted detection and relative density ratio of GSDMD/GSDMD-NT, Pro-IL-1β and caspase1/p-20-caspase1 in cell lysates. (B) IL-1β (n = 6/group) and LDH levels (n = 4/group) in the supernatants. (C) BMDMs were treated with LPS (0.1 μg/ml) + JTE-013 (5 mM) or LPS (0.1 μg/ml) +CYM-5520 (5 mM) for 3 h, followed by ATP treatment (5 mM, 0.5 h). Western blot-assisted detection and relative density ratio of GSDMD/GSDMD-NT, Pro-IL-1β and caspase1/p-20-caspase1 in cell lysates. (D) IL-1β and LDH levels in the supernatants (n = 3/group). (E) Molecular docking of

TβMCA, Gly-βMCA, shows great potential as a therapeutic agent.

The mechanism by which endogenous BAs initiate cholestatic injury through hepatocyte-specific inflammatory responses is compelling.[8] Our study offers new insights into their complex influence on inflammasome activation. Although IPA identified IL-1β as a crucial regulator in both mouse and human IR, the specific effects of BAs on inflammasome function remain unclear since inflammasome activation leads to GSDMD-mediated release of mature IL-1β.[16,17] Notably, if BAs solely stimulated inflammatory responses in hepatocytes, a negative correlation would not be expected between hepatic BA levels and inflammation in the IR models used here. Our findings suggested that IR-induced changes in CYP synthetase expression led to a decrease in TCA concentration and an increase in TβMCA. These BAs yield contrasting effects – promoting or suppressing macrophage pyroptosis. We propose that the conflicting results on BA-mediated inflammasome regulation in past studies stem from the lack of simultaneous assessment of cell death (LDH levels in supernatants).[9,10,19] Indeed, when macrophages were treated with both BAs and inflammasome activators, failing to assay LDH activity could confound the data. Cell death-induced inhibition of inflammasomes might be misinterpreted as inhibition in living cells.[9] This is supported by our observation that TCA upregulated p20-caspase1/GSDMD-NT and supernatant IL-1β levels up to 100 μM, but these levels showed no difference or even decreased at higher concentrations (200 μM) (Fig. S7A,B). Additionally, sustained high LDH levels suggest that inflammasome inhibition might be a consequence of cell death. Furthermore, hydrophobic BAs like CDCA and LCA have shown opposing effects on inflammasomes in different studies.[10,40] Inflammasome activation observed in hydrophobic BA- and LPS-treated cells might be a result of, rather than a cause of, cell death. We observed extensive cell death in CDCA/LPS-treated macrophages, but their morphology differed from LPS/ATP-treated macrophages (Fig. S11A). Moreover, CDCA reduced IL-1β and increased LDH levels in LPS/ATP-treated macrophages (Fig. S11B). Our research findings also indicate that administering a low dose of CDCA before the IR procedure caused more severe liver injury than administering a higher dose (data not shown).

Previous studies have shown that FXR and TGR5 play a role in suppressing inflammasome activation in macrophages. However, in our BDS-IR model, both receptors were suppressed, suggesting other regulatory mechanisms are involved. We focused on S1PR2 as a potential downstream regulator in the BDS-IR model. While the expression of other BARs was similar between BDS-IR and IR models, we observed higher levels of BA hydroxylation enzymes *Cyp2b10* in BDS-IR. This suggests potential activation of CAR and PXR pathways.[41,42] The increase in ASBT (Fig. S2E), BA hydroxylases (Fig. S2B) and OST-β (Figs 1G and 3H) in both IR- and BDS-IR-stressed livers suggests that an adaptive response beyond changes in BA synthesis reduces BA toxicity during reperfusion. Changes in ductular reaction, along with increased ASBT and OST-β expression, lead us to speculate that cholangiocyte proliferation, immune modulation, and the cholehepatic shunt pathway might be involved (Fig. S2C-E).[43–45] In the present study, we focused on how BAs regulate IR-mediated innate immune responses through BARs, particularly the downstream events controlled by the BA-S1PR2 axis. Further studies are warranted to elucidate how IR stress in hepatocytes induces shifts in BA biosynthesis alongside the coordinated induction of adaptive export systems and alternative detoxification enzymes.

Inhibiting GSDMD-NT oligomerization with disulfiram revealed that premature pyroptosis masked the effect of CYM-5520 on caspase-1/GSDMD activation (Fig. S8E-G). Additionally, a high dose of CYM-5520 reduced serum IL-1β and IR injury at 3 h of reperfusion but not at 6 h. This suggests pyroptosis has opposing effects on IRI. These findings support the role of S1PR2 in regulating pyroptosis, which aligns with the effects of BAs on inflammasome modulation. Our findings also offer a potential explanation for the milder inflammatory response observed in myeloid macrophage-specific NLRP3 knock-in mice.[46] Hyperactivated cells tend to produce more IL-1β, whereas pyroptotic cells contribute to a milder phenotype.[15,16] GSDMD determines whether premature pyroptosis leads to a rapid inflammatory response with diminished immune regulation, or sustained IL-1β release from hyperactivated macrophages causing excessive inflammation while maintaining cell viability.[47] This study shows uncoupling of inflammasome activation and cytokine release from immune cells controlled by BAs. It challenges the assumption that pyroptosis always leads to severe inflammatory injury. Further investigation is needed to understand how GSDMD balances immune cell responses at different fates during IR injury.

Molecular docking simulations suggested that BAs share the same binding pocket in S1PR2 as JTE-013/CYM-5520. Since conjugated BAs cannot directly enter immune cells lacking NTCP transporters,[8] TβMCA regulating the downstream pathway by binding to S1PR2 seems like a plausible explanation. Our results demonstrated that TβMCA could inhibit S1PR2 and its downstream signaling. However, the mechanism by which TβMCA reduced S1PR2 expression remains unclear. S1PR2 knockdown effectively prevented the

TβMCA and JTE-013 with S1PR2 was performed using CB-Dock2. The Vina score, location of the binding center, docking size, and interaction residues were evaluated. (F) siControl- or si*S1pr2*-transfected BMDMs were treated with LPS and TβMCA (100 μM and 150 μM) for 3 h, followed by ATP treatment (5 mM, 0.5 h). Western blot-assisted detection and relative density ratio of GSDMD/GSDMD-NT and S1PR2 in cell lysates. (G) IL-1β and LDH levels in supernatants (n = 3/group). (H) BMDMs were treated with LPS (0.1 μg/ml) + JTE-013 (5 mM), LPS (0.1 μg/ml) +CYM-5520 (5 mM), or LPS (0.1 μg/ml) +DMSO for 3 h, followed by ATP treatment (5 mM, 0.5 h). The cell lysates were collected for transcriptomic sequencing and IPA analysis (n = 4/group). (I) DT-pretreated CD11b-DTR mice infused with siControl or si*S1pr2* BMDMs were subjected to IR stress, followed by liver/serum sampling after 6 h of reperfusion (n = 5/group). (J) Serum ALT/AST levels. (K) qRT-PCR-assisted detection of hepatic *S1pr2*. (L) Representative H&E staining of liver sections. Percentages of necrotic areas were quantified (scale bar, 100 μm, 40 μm). (M) qRT-PCR analysis of *Il-1β, Tnf-α, Cxcl1, Cxcl2,* and *Ccl2* levels in the livers. (N) Western blot-assisted detection and relative density ratio of hepatic GSDMD/GSDMD-NT and S1PR2. (O) Serum IL-1β levels. Data are shown as mean±SEM. *p <0.05; **p <0.01; ***p <0.001; ****p <0.0001 by Student's t test or one-way ANOVA analysis. ALT, alanine aminotransferase; AST, aspartate aminotransferase; BAs, bile acids; BMDMs, bone marrow-derived macrophages; DT, diphtheria toxin; IR, ischemia-reperfusion; LDH, lactate dehydrogenase; LPS, lipopolysaccharide; MoMFs, monocyte-derived macrophages; NPCs, non-parenchymal cells; N, necrotic area; qRT-PCR, quantitative reverse-transcription PCR.

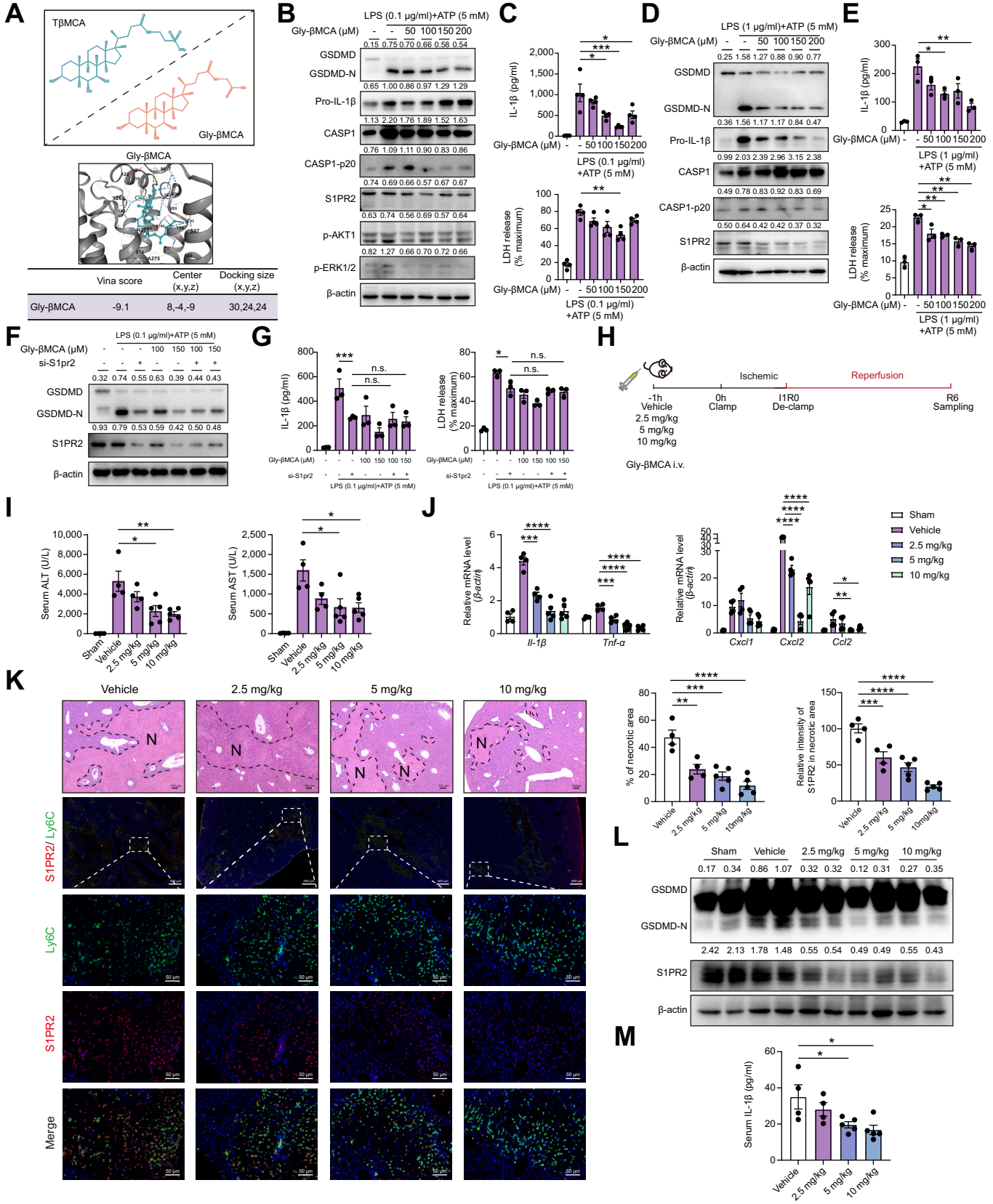

Fig. 7. Gly-βMCA attenuates IR inflammatory injury and inhibits human macrophage pyroptosis. (A) 2D molecular structure of TβMCA and Gly-βMCA and molecular docking results of Gly-βMCA with S1PR2. (B) BMDMs were treated with LPS (0.1 μg/ml) and Gly-βMCA (0, 50, 100, 150 or 200 μM) for 3 h, followed by ATP treatment (5 mM, 0.5 h). Western blot-assisted detection and relative density ratio of GSDMD/GSDMD-NT, Pro-IL-1β, caspase-1/p-20-caspase-1, S1PR2, AKT1, p-AKT1, ERK1/2, and p-ERK1/2 in cell lysates. (C) IL-1β and LDH levels in the supernatants (n = 4/group). (D) THP-1 cells were activated with 50 nM PMA for 48 h and

negative regulation of TβMCA on GSDMD activation in BMDMs, supporting the notion that TβMCA relied primarily on S1PR2 for its regulatory role. Subsequent analysis confirmed that S1PR2 activation could trigger IL-1 family signaling and pyroptotic pathways (Fig. 6H). It also upregulated genes related to the canonical/non-canonical inflammasome pathway, ESCRT-III pathway, mitochondrial damage pathway, and transcriptional regulation in pyroptosis (Fig. S9B). Interestingly, S1PR2 significantly regulated RHO GTPase-related pathways during pyroptosis, which are known to be involved in inflammasome and pyroptosis regulation. These findings collectively support the activating role of S1PR2 in macrophage pyroptosis.

Previous research has shown that pyroptosis in myeloid macrophages can worsen liver damage.[37] We confirmed that S1PR2 on MoMFs exerts a predominantly pro-inflammatory function using immunofluorescence staining, liver-targeted AAV, and a CD11b-DTR adoptive transfer mouse model. This raises the question of whether differences in S1PR2 abundance contribute to the distinct pro-inflammatory capacities of Kupffer cells and MoMFs.[48] Considering that TβMCA reduced hepatic S1PR2 levels (Figs S4J and 5B,C), it is important to explore the role of BAs in neutrophils, given that S1PR2 has been reported to regulate autophagy in neutrophils.[24]

Interestingly, human OLT biopsies showed elevated hepatic *S1pr2* expression without systematic changes in BA synthase. This suggests a potential lack of regulatory mechanisms to repress S1PR2 during the human IR process. Since S1PR2-mediated inflammasome activation has been reported in cholestasis,[23] we examined the correlation between BA metabolic enzymes and S1PR2 expression in the CBDL model. We observed early downregulation of the classical pathway BA synthases *Cyp7a1* and *Cyp8b1* (0-24 h), accompanied by an upregulation of alternative pathway synthases (*Cyp7b1*, *Cyp27a1*, and *Cyp2c70*), as well as upregulation of the phase I hydroxylation enzymes (*Cyp2b10* and *Cyp3a11*) and the phase II conjugation enzymes (*Ugt1a1* and *Sult2a1*). These shifts coincided with the suppression of hepatic S1PR2 expression. At a later stage (7 days), *Cyp7a1* and *Cyp8b1* recovered, while *Cyp7b1*, *Cyp2b10*, *Cyp3a11*, *Ugt1a1*, and *Sult2a1* were suppressed. This appeared to correspond to the upregulation of S1PR2 expression (Fig. S12A-D). Additionally, S1PR2 was predominantly expressed in Ly6C$^+$ MoMFs at different stages of cholestasis (Fig. S12E). We observed distinct phenotypes in the acetaminophen (APAP)-induced liver injury model. A previous study confirmed that APAP could cause a breach of the blood-bile barrier and lead to accumulation of the cytotoxic bile acid TCA in hepatocytes.[30] In contrast to the CBDL and IR models, we observed a significant upregulation of *Cyp8b1*, which mediates TCA production, whereas *Cyp7b1*, *Cyp2c70*, *Cyp2b10*, *Cyp3a11*, and *Ugt1a1* were downregulated (Fig. S13A,B). Interestingly, hepatic S1PR2 expression was markedly upregulated during APAP treatment (Fig. S12C,D). These observations suggest a correlation between shifts in the BA synthase pathway and S1PR2 expression in different liver injury models. Our study extends the understanding that BAs may not act solely as pro-inflammatory factors throughout the entire disease stage, which may correlate with their regulatory role on S1PR2.

In conclusion, this study established the role of TβMCA-S1PR2 signaling, induced by BA metabolic shifts, in regulating myeloid macrophage-specific caspase-1/GSDMD activation. It provided compelling evidence that Gly-βMCA is a promising therapeutic target for liver inflammation.

Affiliations

[1]*Department of Emergency Surgery, Union Hospital, Tongji Medical College, Huazhong University of Science and Technology, Wuhan 430022, China;* [2]*Key Laboratory of Anesthesiology and Resuscitation, Huazhong University of Science and Technology, Ministry of Education, Wuhan 430022, China;* [3]*Department of Medical Genetics, Basic School of Tongji Medical College, Huazhong University of Science and Technology, Wuhan 430030, China;* [4]*Tongji Medical College, Huazhong University of Science and Technology, Wuhan 430030, China;* [5]*Department of Emergency, Union Hospital, Tongji Medical College, Huazhong University of Science and Technology, Wuhan 430022, China;* [6]*Department of Surgery, University of Virginia, Charlottesville, Virginia 22903, USA;* [7]*Center for Translational Medicine, Union Hospital, Tongji Medical College, Huazhong University of Science and Technology, Wuhan 430022, China;* [8]*Department of Hepatobiliary Surgery, Union Hospital, Tongji Medical College, Huazhong University of Science and Technology, Wuhan 430022, China*

Abbreviations

APAP, acetaminophen; BA(s), bile acid(s); BARs, bile acid receptors; BDS-IR, IR model with bile duct separated; BMDMs, bone marrow-derived macrophages; CBA, conjugated bile acid; CBDL, common bile duct ligation; CYP2C70, cytochrome P450 2C70; DEGs, differential expression genes; FXR/NR1H4, farnesoid X receptor; GPBAR1/TGR5, G-protein coupled bile acid receptor 1; Gly-βMCA, glycine-β-muricholic acid; GSDMD, gasdermin D; GSDMD-NT, GSDMD N-terminal fragment; IL-1β, interleukin-1β; IPA, Ingenuity Pathway Analysis; IRI, ischemia-reperfusion injury; LDH, lactate dehydrogenase; LPS, lipopolysaccharide; OLT, orthotopic liver transplantation; MoMFs, monocyte-derived macrophages; PMA, phorbol 12-myristate 13-acetate; S1PR2, sphingosine 1-phosphate receptor 2; TβMCA, tauro-β-muricholic acid.

Financial support

This study was supported by the National Natural Science Foundation of China under grant no. 82170642, no. 82370647, and no. 82100662.

then treated with LPS (1 μg/ml) and Gly-βMCA for 4 h, followed by ATP treatment (5 mM, 0.5 h). Western blot-assisted detection and relative density ratio of GSDMD/GSDMD-NT, pro-IL-1β, caspase-1/p-20-caspase-1, and S1PR2 in cell lysates. (E) IL-1β and LDH levels in supernatants (n = 3/group). (F) siControl- or si*S1pr2*-transfected BMDMs were treated with LPS and Gly-βMCA (100 and 150 μM), followed by ATP treatment (5 mM, 0.5 h). Western blot-assisted detection and relative density ratio of GSDMD/GSDMD-NT and S1PR2 in cell lysates. (G) IL-1β and LDH levels in supernatants (n = 3/group). (H) WT mice were treated with vehicle or different doses of Gly-βMCA (2.5 mg/kg, 5 mg/kg or 10 mg/kg i.v.) 1 h before IR, followed by liver/serum sampling after 6 h of reperfusion (n = 4-5/group). (I) Serum ALT/AST levels. (J) qRT-PCR analysis of *Il-1β, Tnf-α, Cxcl1, Cxcl2,* and *Ccl2* levels in the livers. (K) Representative H&E staining (scale bar, 100 μm) and immunofluorescence staining of Ly6C (green), S1PR2 (red), and merged images in liver sections (original scale bar, 400 μm; magnification scale bar, 50 μm). Percentages of necrotic areas and the intensity of S1PR2 staining were quantified. (L) Western blot-assisted detection and relative density ratio of hepatic GSDMD/GSDMD-NT and S1PR2. (M) Serum IL-1β levels. Data are shown as mean±SEM. *p <0.05; **p <0.01; ***p <0.001; ****p <0.0001 by Student's t test or one-way ANOVA analysis. ALT, alanine aminotransferase; AST, aspartate aminotransferase; BAs, bile acids; BMDMs, bone marrow-derived macrophages; Gly-βMCA, Glycine-beta-muricholic; IPA, Ingenuity Pathway Analysis; IR, ischemia-reperfusion; LDH, lactate dehydrogenase; LPS, lipopolysaccharide; MASH, metabolic dysfunction-associated steatohepatitis; MoMFs, monocyte-derived macrophages; N, necrotic area; OLT, orthotopic liver transplantation; PMA, phorbol 12-myristate 13-acetate; qRT-PCR, quantitative reverse-transcription PCR.

Conflict of interest

The authors declare that they have no conflicts of interest.

Please refer to the accompanying ICMJE disclosure forms for further details.

Authors' contributions

JZ and HW designed and supervised the study; KH, CW, BM, BZ, and TR performed the cell and murine experiments; KH, BM, HZ, and GW operated the surgical procedures; and KH, YG, WP, and GW analyzed transcriptome sequencing data. KH, JL, BM, TR, and XL collected and analyzed public datasets; KH, WP, and PX performed data analysis and interpretation; QZ, XZ, and YZ helped with the flow cytometry experiments; JZ and HW acquired funding; and JZ, HW, JL, KH wrote the manuscript.

Data availability statement

Raw data of transcriptome sequencing with sham liver lobes and ischemic lobes were uploaded to NCBI BioProject and are available with assess code (PRJNA973131, https://www.ncbi.nlm.nih.gov/bioproject/PRJNA973131). One public gene expression dataset (GSE151648, https://www.ncbi.nlm.nih.gov/geo/query/acc.cgi?acc=GSE151648) of human OLT biopsies were used.

Acknowledgements

We thank Dr. Congyi Wang (Huazhong University of Sciences and Technology) for kindly providing the CD11b-DTR mice, as well as for their help with animal experiments.

Supplementary data

Supplementary data to this article can be found online at https://doi.org/10.1016/j.jhepr.2024.101101.

References

Author names in bold designate shared co-first authorship

[1] **Hirao H**, **Nakamura K**, Kupiec-Weglinski JW. Liver ischaemia-reperfusion injury: a new understanding of the role of innate immunity. Nat Rev Gastroenterol Hepatol 2022;19:239–256.
[2] Liu X, Taylor SA, Celaj S, et al. Expression of unfolded protein response genes in post-transplantation liver biopsies. BMC Gastroenterol 2022;22:380.
[3] Bernhardt GA, Zollner G, Cerwenka H, et al. Hepatobiliary transporter expression and post-operative jaundice in patients undergoing partial hepatectomy. Liver Int 2012;32:119–127.
[4] Buis CI, Geuken E, Visser DS, et al. Altered bile composition after liver transplantation is associated with the development of nonanastomotic biliary strictures. J Hepatol 2009;50:69–79.
[5] Georgiev P, Navarini AA, Eloranta JJ, et al. Cholestasis protects the liver from ischaemic injury and post-ischaemic inflammation in the mouse. Gut 2007;56:121–128.
[6] **Zhu C**, **Boucheron N**, Muller AC, et al. 24-Norursodeoxycholic acid reshapes immunometabolism in CD8(+) T cells and alleviates hepatic inflammation. J Hepatol 2021;75:1164–1176.
[7] Fuchs CD, Trauner M. Role of bile acids and their receptors in gastrointestinal and hepatic pathophysiology. Nat Rev Gastroenterol Hepatol 2022;19:432–450.
[8] Cai SY, Ouyang X, Chen Y, et al. Bile acids initiate cholestatic liver injury by triggering a hepatocyte-specific inflammatory response. JCI Insight 2017;2:e90780.
[9] **Guo C**, **Xie S**, **Chi Z**, et al. Bile acids control inflammation and metabolic disorder through inhibition of NLRP3 inflammasome. Immunity 2016;45:944.
[10] **Hao H**, **Cao L**, **Jiang C**, et al. Farnesoid X receptor regulation of the NLRP3 inflammasome underlies cholestasis-associated sepsis. Cell Metab. 2017;25:856–867 e5.
[11] Kagan JC, Magupalli VG, Wu H. SMOCs: supramolecular organizing centres that control innate immunity. Nat Rev Immunol 2014;14:821–826.
[12] Huang H, Chen HW, Evankovich J, et al. Histones activate the NLRP3 inflammasome in Kupffer cells during sterile inflammatory liver injury. J Immunol 2013;191:2665–2679.
[13] Kamo N, Ke B, Ghaffari AA, et al. ASC/caspase-1/IL-1beta signaling triggers inflammatory responses by promoting HMGB1 induction in liver ischemia/reperfusion injury. Hepatology 2013;58:351–362.
[14] **Xu B**, **Jiang M**, **Chu Y**, et al. Gasdermin D plays a key role as a pyroptosis executor of non-alcoholic steatohepatitis in humans and mice. J Hepatol 2018;68:773–782.
[15] Devant P, Kagan JC. Molecular mechanisms of gasdermin D pore-forming activity. Nat Immunol 2023;24:1064–1075.
[16] Xia S, Zhang Z, Magupalli VG, et al. Gasdermin D pore structure reveals preferential release of mature interleukin-1. Nature 2021;593:607–611.
[17] Evavold CL, Ruan J, Tan Y, et al. The pore-forming protein gasdermin D regulates interleukin-1 secretion from living macrophages. Immunity 2018;48:35–44 e6.
[18] **Shi J**, **Zhao Y**, Wang K, et al. Cleavage of GSDMD by inflammatory caspases determines pyroptotic cell death. Nature 2015;526:660–665.
[19] Cai SY, Ge M, Mennone A, et al. Inflammasome is activated in the liver of cholestatic patients and aggravates hepatic injury in bile duct-ligated mouse. Cell Mol Gastroenterol Hepatol 2020;9:679–688.
[20] **Che Y**, **Xu W**, **Ding C**, et al. Bile acids target mitofusin 2 to differentially regulate innate immunity in physiological versus cholestatic conditions. Cell Rep. 2023;42:112011.
[21] **Studer E**, **Zhou X**, **Zhao R**, et al. Conjugated bile acids activate the sphingosine-1-phosphate receptor 2 in primary rodent hepatocytes. Hepatology 2012;55:267–276.
[22] **Wang Y**, **Aoki H**, **Yang J**, et al. The role of sphingosine 1-phosphate receptor 2 in bile-acid-induced cholangiocyte proliferation and cholestasis-induced liver injury in mice. Hepatology 2017;65:2005–2018.
[23] Hou L, Yang L, Chang N, et al. Macrophage sphingosine 1-phosphate receptor 2 blockade attenuates liver inflammation and fibrogenesis triggered by NLRP3 inflammasome. Front Immunol 2020;11:1149.
[24] **Hirao H**, **Kojima H**, Dery KJ, et al. Neutrophil CEACAM1 determines susceptibility to NETosis by regulating the S1PR2/S1PR3 axis in liver transplantation. J Clin Invest 2023;133.
[25] **Chen L**, **Jiao T**, **Liu W**, et al. Hepatic cytochrome P450 8B1 and cholic acid potentiate intestinal epithelial injury in colitis by suppressing intestinal stem cell renewal. Cell Stem Cell 2022;29:1366–1381 e9.
[26] Jia W, Wei M, Rajani C, et al. Targeting the alternative bile acid synthetic pathway for metabolic diseases. Protein Cell 2021;12:411–425.
[27] Sosa RA, Terry AQ, Kaldas FM, et al. Disulfide high-mobility group box 1 drives ischemia-reperfusion injury in human liver transplantation. Hepatology 2021;73:1158–1175.
[28] **Pan WM**, **Wang H**, Zhang XF, et al. miR-210 participates in hepatic ischemia reperfusion injury by forming a negative feedback loop with SMAD4. Hepatology 2020;72:2134–2148.
[29] Ballatori N, Christian WV, Lee JY, et al. OSTalpha-OSTbeta: a major basolateral bile acid and steroid transporter in human intestinal, renal, and biliary epithelia. Hepatology 2005;42:1270–1279.
[30] Ghallab A, Hassan R, Hofmann U, et al. Interruption of bile acid uptake by hepatocytes after acetaminophen overdose ameliorates hepatotoxicity. J Hepatol 2022;77:71–83.
[31] Takahashi S, Fukami T, Masuo Y, et al. Cyp2c70 is responsible for the species difference in bile acid metabolism between mice and humans. J Lipid Res 2016;57:2130–2137.
[32] **de Boer JF**, **Verkade E**, Mulder NL, et al. A human-like bile acid pool induced by deletion of hepatic Cyp2c70 modulates effects of FXR activation in mice. J Lipid Res 2020;61:291–305.
[33] Li R, Hovingh MV, Koehorst M, et al. Short-term obeticholic acid treatment does not impact cholangiopathy in Cyp2c70-deficient mice with a human-like bile acid composition. Biochim Biophys Acta Mol Cell Biol Lipids 2022;1867:159163.
[34] Guillot A, Tacke F. Liver macrophages: old dogmas and new insights. Hepatol Commun 2019;3:730–743.
[35] **Hu JJ**, **Liu X**, Xia S, et al. FDA-approved disulfiram inhibits pyroptosis by blocking gasdermin D pore formation. Nat Immunol 2020;21:736–745.
[36] Liu Y, Yang X, Gan J, et al. CB-Dock2: improved protein-ligand blind docking by integrating cavity detection, docking and homologous template fitting. Nucleic Acids Res 2022;50:W159–W164.
[37] Kadono K, Kageyama S, Nakamura K, et al. Myeloid Ikaros-SIRT1 signaling axis regulates hepatic inflammation and pyroptosis in ischemia-stressed mouse and human liver. J Hepatol 2022;76:896–909.
[38] **Jiang J**, **Ma Y**, Liu Y, et al. Glycine-beta-muricholic acid antagonizes the intestinal farnesoid X receptor-ceramide axis and ameliorates NASH in mice. Hepatol Commun 2022;6:3363–3378.
[39] **Jiang C**, **Xie C**, Lv Y, et al. Intestine-selective farnesoid X receptor inhibition improves obesity-related metabolic dysfunction. Nat Commun 2015;6:10166.

[40] **Gong Z**, **Zhou J**, **Zhao S**, et al. Chenodeoxycholic acid activates NLRP3 inflammasome and contributes to cholestatic liver fibrosis. Oncotarget 2016;7:83951–83963.
[41] Wagner M, Halilbasic E, Marschall HU, et al. CAR and PXR agonists stimulate hepatic bile acid and bilirubin detoxification and elimination pathways in mice. Hepatology 2005;42:420–430.
[42] Stedman CA, Liddle C, Coulter SA, et al. Nuclear receptors constitutive androstane receptor and pregnane X receptor ameliorate cholestatic liver injury. Proc Natl Acad Sci U S A. 2005;102:2063–2068.
[43] Guillot A, Guerri L, Feng D, et al. Bile acid-activated macrophages promote biliary epithelial cell proliferation through integrin αvβ6 upregulation following liver injury. J Clin Invest 2021;131(9):e132305.
[44] **Banales JM**, **Huebert RC**, **Karlsen T**, et al. Cholangiocyte pathobiology. Nat Rev Gastroenterol Hepatol 2019;16(5):269–281.
[45] **Xia X**, **Francis H**, **Glaser S**, et al. Bile acid interactions with cholangiocytes. World J Gastroenterol 2006;12(22):3553–3563.
[46] Wree A, Eguchi A, McGeough MD, et al. NLRP3 inflammasome activation results in hepatocyte pyroptosis, liver inflammation, and fibrosis in mice. Hepatology 2014;59:898–910.
[47] **Carty M**, **Kearney J**, Shanahan KA, et al. Cell survival and cytokine release after inflammasome activation is regulated by the toll-IL-1R protein SARM. Immunity 2019;50:1412–1424 e6.
[48] **Zigmond E**, **Samia-Grinberg S**, Pasmanik-Chor M, et al. Infiltrating monocyte-derived macrophages and resident kupffer cells display different ontogeny and functions in acute liver injury. J Immunol 2014;193:344–353.

Keywords: S1PR2; Pyroptosis; CYP2C70; GSDMD; Liver transplantation; Macrophages.
Received 26 October 2023; received in revised form 10 April 2024; accepted 16 April 2024; Available online 25 April 2024